PHYSICAL REVIEW D **86,** 075013 (2012)

Constraining anomalous Higgs boson interactions

Tyler Corbett[*]
C.N. Yang Institute for Theoretical Physics, SUNY at Stony Brook, Stony Brook, New York 11794-3840, USA

O. J. P. Éboli[†]
Instituto de Física, Universidade de São Paulo, Caixa Postal 66318, CEP 05314-970 São Paulo, Brazil and Institut de Physique Théorique, CEA-Saclay Orme des Merisiers, 91191 Gif-sur-Yvette, France

J. Gonzalez-Fraile[‡]
Departament d'Estructura i Constituents de la Matèria and ICC-UB, Universitat de Barcelona, 647 Diagonal, E-08028 Barcelona, Spain

M. C. Gonzalez-Garcia[§]
C.N. Yang Institute for Theoretical Physics, SUNY at Stony Brook, Stony Brook, New York 11794-3840, USA Institució Catalana de Recerca i Estudis Avançats (ICREA), and Departament d'Estructura i Constituents de la Matèria, Universitat de Barcelona, 647 Diagonal, E-08028 Barcelona, Spain
(Received 19 July 2012; published 9 October 2012)

The recently announced Higgs boson discovery marks the dawn of the direct probing of the electroweak symmetry breaking sector. Sorting out the dynamics responsible for electroweak symmetry breaking now requires probing the Higgs boson interactions and searching for additional states connected to this sector. In this work, we analyze the constraints on Higgs boson couplings to the standard model gauge bosons using the available data from Tevatron and LHC. We work in a model-independent framework expressing the departure of the Higgs boson couplings to gauge bosons by dimension-six operators. This allows for independent modifications of its couplings to gluons, photons, and weak gauge bosons while still preserving the Standard Model (SM) gauge invariance. Our results indicate that best overall agreement with data is obtained if the cross section of Higgs boson production via gluon fusion is suppressed with respect to its SM value and the Higgs boson branching ratio into two photons is enhanced, while keeping the production and decays associated to couplings to weak gauge bosons close to their SM prediction.

DOI: 10.1103/PhysRevD.86.075013 PACS numbers: 14.80.Bn, 12.60.Fr, 14.80.Ec

I. INTRODUCTION

The electroweak symmetry breaking (EWSB) mechanism has been elusive for many decades. However the recently announced discovery of a 125 GeV Higgs boson [1–6] at the CERN Large Hadron Collider (LHC) [7,8] opens a new era in particle physics. The pressing questions now are related to the properties of this new observed state, such as its spin and couplings, in order to extend our knowledge of the EWSB sector. In this work we employ the data used for the Higgs boson discovery to constrain its couplings to gauge bosons.

Presently, there are many possible EWSB scenarios ranging from the Higgs boson being elementary and weakly interacting [9], as in the Standard Model (SM), to it being composite and related to a new strongly interacting sector [10,11]. In this last case the precision electroweak measurements and flavor changing neutral currents lead to strong constraints. However, recent theoretical advances have made possible the construction of models in agreement with the experimental bounds [12]. The distinction between the different scenarios can be carried out by looking for further new states associated with the EWSB mechanism and/or by careful studies of the Higgs boson couplings.

In this work we assume that the observed Higgs boson is part of a $SU(2)_L$ doublet and that possible additional states are heavy enough not to play a direct role in the low-energy phenomenology. This assumption is realized in models where the Higgs boson is a pseudo-Goldstone boson of a larger broken global symmetry [13–19]. Under this assumption, we consider the most general dimension-six effective Lagrangian invariant under linear $SU(3)_c \otimes SU(2)_L \otimes U(1)_Y$ transformations to describe the interactions of the Higgs boson with the electroweak gauge bosons, as well as with the gluons [20,21]. For the sake of simplicity we assume that the Higgs boson has the same interaction with fermions as in the SM; nevertheless, this hypothesis still has to be tested further.[1] This scenario can be falsified by the discovery of new states or by the

[*]corbett.ts@gmail.com
[†]eboli@fma.if.usp.br
[‡]fraile@ecm.ub.es
[§]concha@insti.physics.sunysb.edu

[1]The preliminary CMS [8] results indicate that the SM values for the Higgs boson couplings to fermions are within the 90–95% CL allowed region.

nonobservation of its predictions to the triple electroweak gauge boson vertices.

The effective operators describing the Higgs boson anomalous interactions modify both the Higgs boson production mechanisms and its decay patterns; therefore, we combine several channels to unravel the contribution of the different operators. In our analyses we use the most recent data from the Tevatron [22] and LHC at 7 TeV [23,24] and at 8 TeV [7,8,25–27]. Anomalous interactions also enhance the Higgs boson decay into $Z\gamma$ as well as its production in association with a photon. Nevertheless, the available statistics is not enough to make these channels visible.

This article is organized as follows. In Sec. II we introduce the dimension-six effective operators and the different scenarios studied in this work. Details of our analyses are presented in Secs. III and IV, contains their results. Finally we discuss the main conclusions in Sec. V.

II. HIGGS BOSON ANOMALOUS INTERACTIONS

In this work we assume that even if there is new physics associated with the electroweak symmetry breaking sector, the Higgs boson observed at LHC is still part of a $SU(2)_L$ doublet, the SM gauge invariance holds, and no additional light states, relevant to the Higgs boson observables, are present in the spectrum. Under these assumptions, the new effects can be parametrized in a model-independent way by extending the SM with the addition of higher dimension operators that are invariant under linear $SU(3)_c \otimes SU(2)_L \otimes U(1)_Y$ transformations.

In this framework, the first corrections to the Higgs boson couplings to gauge bosons are expressed as dimension-six operators that can be written as

$$\mathcal{L}_{\text{eff}} = \sum_n \frac{f_n}{\Lambda^2}\mathcal{O}_n, \tag{1}$$

where the operators $\mathcal{O}_n$ involve vector boson and/or Higgs boson fields with couplings f_n and where Λ is a characteristic scale. Requiring the operators $\mathcal{O}_n$ to be P and C even, there are only seven dimension-six operators that modify the Higgs boson couplings to electroweak vector bosons and one to gluons [20,21]:

$$\begin{aligned}
\mathcal{O}_{GG} &= \Phi^\dagger\Phi G^a_{\mu\nu}G^{a\mu\nu},\\
\mathcal{O}_{WW} &= \Phi^\dagger\hat{W}_{\mu\nu}\hat{W}^{\mu\nu}\Phi,\\
\mathcal{O}_{BB} &= \Phi^\dagger\hat{B}_{\mu\nu}\hat{B}^{\mu\nu}\Phi,\\
\mathcal{O}_{BW} &= \Phi^\dagger\hat{B}_{\mu\nu}\hat{W}^{\mu\nu}\Phi,\\
\mathcal{O}_{W} &= (D_\mu\Phi)^\dagger\hat{W}^{\mu\nu}(D_\nu\Phi),\\
\mathcal{O}_{B} &= (D_\mu\Phi)^\dagger\hat{B}^{\mu\nu}(D_\nu\Phi),\\
\mathcal{O}_{\Phi,1} &= (D_\mu\Phi)^\dagger\Phi^\dagger\Phi(D^\mu\Phi),\\
\mathcal{O}_{\Phi,2} &= \frac{1}{2}\partial^\mu(\Phi^\dagger\Phi)\partial_\mu(\Phi^\dagger\Phi),
\end{aligned} \tag{2}$$

where Φ stands for the Higgs boson doublet, D_μ is the covariant derivative, $\hat{B}_{\mu\nu} = i(g'/2)B_{\mu\nu}$, and $\hat{W}_{\mu\nu} = i(g/2)\sigma^a W^a_{\mu\nu}$, with $B_{\mu\nu}$, $W^a_{\mu\nu}$, and $G^a_{\mu\nu}$ being, respectively, the $U(1)_Y$, $SU(2)_L$, and $SU(3)_c$ field strength tensors. We denote the $SU(2)_L$ $[U(1)_Y]$ gauge coupling as g $[g']$ and the Pauli matrices as σ^a.

The effective operators in Eq. (2) give rise to anomalous Hgg, $H\gamma\gamma$, $HZ\gamma$, HZZ, and HW^+W^- couplings, which in the unitary gauge are given by

$$\begin{aligned}
\mathcal{L}^{\text{HVV}}_{\text{eff}} = {}& g_{Hgg}HG^a_{\mu\nu}G^{a\mu\nu} + g_{H\gamma\gamma}HA_{\mu\nu}A^{\mu\nu}\\
&+ g^{(1)}_{HZ\gamma}A_{\mu\nu}Z^\mu\partial^\nu H + g^{(2)}_{HZ\gamma}HA_{\mu\nu}Z^{\mu\nu}\\
&+ g^{(1)}_{HZZ}Z_{\mu\nu}Z^\mu\partial^\nu H + g^{(2)}_{HZZ}HZ_{\mu\nu}Z^{\mu\nu}\\
&+ g^{(3)}_{HZZ}HZ_\mu Z^\mu + g^{(1)}_{HWW}(W^+_{\mu\nu}W^{-\mu}\partial^\nu H + \text{H.c.})\\
&+ g^{(2)}_{HWW}HW^+_{\mu\nu}W^{-\mu\nu} + g^{(3)}_{HWW}HW^+_\mu W^{-\mu},
\end{aligned} \tag{3}$$

where $V_{\mu\nu} = \partial_\mu V_\nu - \partial_\nu V_\mu$ with $V = A$, Z, and W. The effective couplings g_{Hgg}, $g_{H\gamma\gamma}$, $g^{(1,2)}_{HZ\gamma}$, $g^{(1,2,3)}_{HWW}$, and $g^{(1,2,3)}_{HZZ}$ are related to the coefficients of the operators appearing in (1) through

$$\begin{aligned}
g_{Hgg} &= \frac{f_{GG}v}{\Lambda^2} \equiv -\frac{\alpha_s}{8\pi}\frac{f_g v}{\Lambda^2},\\
g_{H\gamma\gamma} &= -\left(\frac{gM_W}{\Lambda^2}\right)\frac{s^2(f_{BB}+f_{WW}-f_{BW})}{2},\\
g^{(1)}_{HZ\gamma} &= \left(\frac{gM_W}{\Lambda^2}\right)\frac{s(f_W-f_B)}{2c},\\
g^{(2)}_{HZ\gamma} &= \left(\frac{gM_W}{\Lambda^2}\right)\frac{s[2s^2f_{BB}-2c^2f_{WW}+(c^2-s^2)f_{BW}]}{2c},\\
g^{(1)}_{HZZ} &= \left(\frac{gM_W}{\Lambda^2}\right)\frac{c^2f_W+s^2f_B}{2c^2},\\
g^{(2)}_{HZZ} &= -\left(\frac{gM_W}{\Lambda^2}\right)\frac{s^4f_{BB}+c^4f_{WW}+c^2s^2f_{BW}}{2c^2},\\
g^{(3)}_{HZZ} &= \left(\frac{gM_Wv^2}{\Lambda^2}\right)\frac{f_{\Phi,1}-f_{\Phi,2}}{4c^2},\\
g^{(1)}_{HWW} &= \left(\frac{gM_W}{\Lambda^2}\right)\frac{f_W}{2},\\
g^{(2)}_{HWW} &= -\left(\frac{gM_W}{\Lambda^2}\right)f_{WW},\\
g^{(3)}_{HWW} &= -\left(\frac{gM_Wv^2}{\Lambda^2}\right)\frac{f_{\Phi,1}+2f_{\Phi,2}}{4},
\end{aligned} \tag{4}$$

where s and c stand for the sine and cosine of the weak mixing angle, respectively. We notice that we have rescaled the coefficient f_{GG} of the gluon-gluon operator in terms of a coupling f_g, also including a loop suppression factor. In this way an anomalous gluon-gluon coupling $f_g \sim \mathcal{O}(1\text{–}10)$ gives a contribution comparable to the SM top loop. For the operators involving electroweak gauge bosons, we have kept the normalization commonly used in

the pre-LHC studies, for example, in Refs. [28–32]. The couplings $g^{(3)}_{HZZ}$ and $g^{(3)}_{HWW}$ include the effects arising from the contribution of the operators $\mathcal{O}_{\Phi,1}$ and $\mathcal{O}_{\Phi,2}$ to the renormalization of the weak boson masses and the Higgs boson field wave function.

For the sake of concreteness in this work, we focus our attention on modifications of the Higgs boson couplings to gauge bosons associated with the five operators $\mathcal{O}_{GG}$, $\mathcal{O}_{BB}$, $\mathcal{O}_{WW}$, $\mathcal{O}_B$, and $\mathcal{O}_W$. The operator $\mathcal{O}_{BW}$ contributes at tree level to the W^3-B mixing and is therefore very strongly constrained by the electroweak precision data [28,29,33,34]. Similarly, $\mathcal{O}_{\Phi,1}$ contributes to the Z mass but not to the W mass and it is severely constrained by the ρ parameter. Moreover, the operators $\mathcal{O}_{\Phi,1}$ and $\mathcal{O}_{\Phi,2}$ lead to a multiplicative contribution to the SM Higgs boson couplings to ZZ and WW. Thus, in the present analysis we do not consider effects associated with $\mathcal{O}_{BW}$, $\mathcal{O}_{\Phi,1}$, and $\mathcal{O}_{\Phi,2}$ since their coefficients are already very constrained or their possible effect on the measured Higgs boson observables is degenerated with that of the five operators considered. Their impact on the Higgs boson phenomenology can be seen in Refs. [8,35–41].

Notice also that one expects the contribution of new physics to the five operators considered to take place at loop level [42]. Therefore, we expect that the largest effect of these effective interactions should appear in the couplings of the Higgs boson to photon-photon and gluon-gluon since these couplings take place through loop effects in the SM.

One important property of the operators $\mathcal{O}_B$ and $\mathcal{O}_W$ is that they also modify the triple gauge boson couplings γW^+W^- and ZW^+W^-. Consequently, they can be directly probed in additional channels not directly involving the Higgs boson [31,43,44]. The triple gauge boson effective interaction can be rewritten in the standard parametrization of the C and P even interactions [45]:

$$\mathcal{L}_{WWV} = -ig_{WWV}\Big\{g_1^V(W^+_{\mu\nu}W^{-\mu}V^{\nu} - W^+_{\mu}V_{\nu}W^{-\mu\nu}) + \kappa_V W^+_{\mu}W^-_{\nu}V^{\mu\nu} + \frac{\lambda_V}{m_W^2}W^+_{\mu\nu}W^{-\nu\rho}V^{\mu}_{\rho}\Big\}, \tag{5}$$

where $g_{WW\gamma} = e$ and $g_{WWZ} = e/(sc)$. In general these vertices involve six dimensionless couplings g_1^V, κ_V, and λ_V ($V = \gamma$ or Z). Notwithstanding, the electromagnetic gauge invariance requires that $g_1^{\gamma} = 1$, while the remaining five free couplings are related to the dimension-six operators that we are considering:

$$\begin{aligned}
\Delta g_1^Z &= g_1^Z - 1 = \frac{1}{2}\frac{m_Z^2}{\Lambda^2}f_W, \\
\Delta\kappa_{\gamma} &= \kappa_{\gamma} - 1 = \frac{1}{2}\frac{m_W^2}{\Lambda^2}(f_W + f_B), \\
\Delta\kappa_Z &= \kappa_Z - 1 = \frac{1}{2}\frac{m_Z^2}{\Lambda^2}(c^2 f_W - s^2 f_B), \\
\lambda_{\gamma} &= \lambda_Z = 0.
\end{aligned} \tag{6}$$

In summary, in the theoretical framework that we are using, the observables depend upon five parameters: f_g, f_B, f_W, f_{BB}, and f_{WW}. In what follows for the sake of simplicity we focus on two different scenarios:

(i) *Scenario I:* We impose that $f_W = f_B$ and $f_{BB} = f_{WW}$. This scenario has three free parameters (f_W, f_{WW}, and f_g) and it exhibits a constraint between the three couplings of the Higgs boson to electroweak vector bosons. This scenario predicts the existence of anomalous triple electroweak gauge boson interactions.

(ii) *Scenario II:* We set $f_W = f_B = 0$ and $f_{WW} = f_{BB}$. This scenario has two free parameters (f_g and $f_{BB} = f_{WW}$) and it can be considered the low-energy limit of an extension of the SM that contains an extra heavy scalar multiplet; for details, see Ref. [34]. Moreover, this scenario cannot be constrained by data on triple gauge boson couplings.

The above relations (6) allow us to constrain the couplings f_B and f_W using the available experimental bounds on the effective couplings Δg_1^Z, $\Delta\kappa_{\gamma}$, and $\Delta\kappa_Z$ [46]. Nevertheless, these experimental bounds are usually obtained assuming only one anomalous operator different from the SM value at a time, an assumption which is not consistent with our scenario I. For this reason, strictly speaking, one cannot apply the exclusion limits in Ref. [46] to this scenario. Nevertheless, if we assume no strong cancellations among the contributions of the different triple gauge-effective operators, we can estimate the size of the exclusion limits on f_W and f_B. Using the 95% CL regions from Ref. [46] on Δg_1^Z, $\Delta\kappa_{\gamma}$, or $\Delta\kappa_Z$ we obtain that in scenario I the 95% CL regions on $f_W = f_B$ are $[-13, 7]\ \mathrm{TeV}^{-2}$, $[-18, 9]\ \mathrm{TeV}^{-2}$, and $[-85, 20]\ \mathrm{TeV}^{-2}$, respectively. Notice also that LHC already with present runs has potential to constrain the triple gauge boson vertices [47] and the collaborations are starting to look for deviations [43,44]. However, at present, their individual limits have not reached the level of the LEP bounds yet.

III. ANALYSIS FRAMEWORK

In order to obtain the present constraints on the Higgs boson anomalous interactions, we perform a chi-square test using the available data on the signal strength (μ) from Tevatron, LHC at 7 TeV, and LHC at 8 TeV. We assume that the correlations among the different channels are negligible except for the theoretical uncertainties which are treated with the pull method [48,49] in order to account for their correlations.

Schematically we can write

$$\chi^2 = \min_{\xi_{\mathrm{pull}}} \sum_j \frac{(\mu_j - \mu_j^{\mathrm{exp}})^2}{\sigma_j^2} + \sum_{\mathrm{pull}} \left(\frac{\xi_{\mathrm{pull}}}{\sigma_{\mathrm{pull}}}\right)^2, \tag{7}$$

TABLE I. Processes considered in our analyses for the LHC 7 TeV run and for the Tevatron. We present the errors and best fit point for the signal strength for each topology.

Channel	$\mu^{\exp}$	Comment
$p\bar{p} \to W^+W^-$	$0.3^{+1.1}_{-0.3}$	CDF and DØ [22]
$p\bar{p} \to b\bar{b}$	$2.0^{+0.7}_{-0.7}$	CDF and DØ [22]
$p\bar{p} \to \gamma\gamma$	$3.6^{+3.0}_{-2.5}$	CDF and DØ [22]
$pp \to \tau\bar{\tau}$	$0.2^{+1.7}_{-1.9}$	ATLAS [23]
$pp \to b\bar{b}$	$0.5^{+2.1}_{-2.0}$	ATLAS [23]
$pp \to ZZ^* \to \ell^+\ell^-\ell^+\ell^-$	$1.4^{+1.3}_{-0.8}$	ATLAS [23]
$pp \to WW^* \to \ell^+\nu\ell^-\bar{\nu}$	$0.5^{+0.6}_{-0.6}$	ATLAS [23]
$pp \to \gamma\gamma$	$2.2^{+0.8}_{-0.8}$	ATLAS [27]
$pp \to \tau\bar{\tau}$	$0.6^{+1.1}_{-1.2}$	CMS [24]
$pp \to b\bar{b}$	$0.5^{+1.1}_{-1.0}$	CMS [26]
$pp \to ZZ^* \to \ell^+\ell^-\ell^+\ell^-$	$0.6^{+0.9}_{-0.6}$	CMS [24]
$pp \to WW^* \to \ell^+\nu\ell^-\bar{\nu}$	$0.4^{+0.6}_{-0.6}$	CMS [24]
$pp \to \gamma\gamma$ Untagged 0	$3.2^{+1.9}_{-1.8}$	CMS [25]
$pp \to \gamma\gamma$ Untagged 1	$0.7^{+0.9}_{-1.0}$	CMS [25]
$pp \to \gamma\gamma$ Untagged 2	$0.7^{+1.2}_{-1.1}$	CMS [25]
$pp \to \gamma\gamma$ Untagged 3	$1.5^{+1.6}_{-1.6}$	CMS [25]
$pp \to \gamma\gamma jj$	$4.2^{+2.0}_{-2.0}$	CMS [25]

TABLE II. Available data including the 8 TeV run. We present the errors and best fit point for the signal strength for each channel. The data that have been combined are indicated as "@ 7 and 8 TeV.".

Channel	$\mu^{\exp}$	Comment
$pp \to ZZ^* \to \ell^+\ell^-\ell^+\ell^-$	$1.3^{+0.6}_{-0.6}$	ATLAS @ 7 and 8 TeV [7]
$pp \to \gamma\gamma$	$1.8^{+0.6}_{-0.7}$	ATLAS [27]
$pp \to \tau\bar{\tau}$	$-0.2^{+0.8}_{-0.7}$	CMS @ 7 and 8 TeV [8]
$pp \to b\bar{b}$	$0.4^{+0.9}_{-0.8}$	CMS [26]
$pp \to ZZ^* \to \ell^+\ell^-\ell^+\ell^-$	$0.7^{+0.6}_{-0.4}$	CMS [26]
$pp \to WW^* \to \ell^+\nu\ell^-\bar{\nu}$	$0.6^{+0.4}_{-0.4}$	CMS @ 7 and 8 TeV [8]
$pp \to \gamma\gamma$ Untagged 0	$1.5^{+1.2}_{-1.2}$	CMS [25]
$pp \to \gamma\gamma$ Untagged 1	$1.5^{+1.0}_{-1.0}$	CMS [25]
$pp \to \gamma\gamma$ Untagged 2	$1.0^{+1.1}_{-1.2}$	CMS [25]
$pp \to \gamma\gamma$ Untagged 3	$3.8^{+1.7}_{-1.8}$	CMS [25]
$pp \to \gamma\gamma jj$ loose	$-0.6^{+2.1}_{-2.0}$	CMS [25]
$pp \to \gamma\gamma jj$ tight	$1.3^{+1.5}_{-1.6}$	CMS [25]

where j stands for channels presented in Tables I and II. We denote the theoretically expected signal as μ_j, the observed best fit values as $\mu_j^{\exp}$, and errors as $\sigma_j^{+,-}$. As we can see from these tables, the errors are not symmetric, showing a deviation from a Gaussian behavior as expected from the still low statistics. In our calculations we make the errors in each channel symmetric by taking

$$\sigma_j = \sqrt{\frac{(\sigma_j^+)^2 + (\sigma_j^-)^2}{2}}. \tag{8}$$

Concerning the theoretical uncertainties, the largest are associated with the gluon fusion subprocess. To account for these errors, we introduce two pull factors: one for the Tevatron (ξ_T) and one for the LHC at 7 and 8 TeV (ξ_L). They modify the corresponding predictions as shown in Eqs. (12) and (13). We consider that the errors associated with the pulls are $\sigma_T = 0.4$ and $\sigma_L = 0.15$. As statistics build up, it will be necessary to introduce pulls associated with the theoretical uncertainties for the other production mechanisms, as well as possible systematic correlated errors; however, at this moment, these are subleading effects.

TABLE III. Weight of each production mechanism for the different $\gamma\gamma$ categories in the CMS analyses of the 7 TeV data.

Channel	ϵ_{gg}	$\epsilon_{\rm VBF}$	$\epsilon_{\rm VH}$	$\epsilon_{t\bar{t}H}$
$pp \to \gamma\gamma$ Untagged 0	0.13	0.46	0.70	1
$pp \to \gamma\gamma$ Untagged 1	0.57	0.49	0.67	1
$pp \to \gamma\gamma$ Untagged 2	1	0.56	0.76	0
$pp \to \gamma\gamma$ Untagged 3	1	0.56	0.76	0
$pp \to \gamma\gamma jj$	0.029	1	0.019	0

TABLE IV. Same as Table III but for the 8 TeV CMS data.

Channel	ϵ_{gg}	$\epsilon_{\rm VBF}$	$\epsilon_{\rm VH}$	$\epsilon_{t\bar{t}H}$
$pp \to \gamma\gamma$ Untagged 0	0.11	0.25	0.48	1
$pp \to \gamma\gamma$ Untagged 1	0.59	0.50	0.72	1
$pp \to \gamma\gamma$ Untagged 2	1	0.54	0.58	0
$pp \to \gamma\gamma$ Untagged 3	1	0.54	0.78	0
$pp \to \gamma\gamma jj$ loose	0.094	1	0.064	0
$pp \to \gamma\gamma jj$ tight	0.024	1	0	0

One important approximation in our analyses is that we neglect the effects associated with the distortions of the kinematical distributions of the final states due to the Higgs boson anomalous couplings arising from their non SM-like Lorentz structure. Thus we implicitly assume that the anomalous contributions have the same detection efficiencies as the SM Higgs boson. A full simulation of the Higgs boson anomalous operators taking advantage of their special kinematical features would increase the current sensitivity on the anomalous couplings. It would also allow for breaking degeneracies with those operators which only lead to an overall modification of strength of the SM vertices. But at present, there is not enough public information to perform such analysis outside of the experimental collaborations.

In order to predict the modification of the observables, we need to include the effect of the anomalous operators in the production channels as well as in the decay branching ratios. At this time, the evaluation of all cross sections containing anomalous Higgs boson couplings is not available in the literature; therefore, we assumed, as a first approximation, that the K factor associated with higher order corrections is the same for the SM and anomalous contributions.[2] We write

$$\sigma_Y^{\rm ano} = \frac{\sigma_Y^{\rm ano}}{\sigma_Y^{\rm SM}}\Big|_{\rm tree} \sigma_Y^{\rm SM}|_{\rm soa}, \tag{9}$$

where the ratio of the anomalous and SM cross sections of the subprocess Y ($= gg$, VBF, VH, or $t\bar{t}H$) is evaluated at tree level and it is multiplied by the value for the state-of-the-art SM cross section calculations ($\sigma_Y^{\rm SM}|_{\rm soa}$) presented in Ref. [50]. Analogously, we write the decay width into the final state X as

$$\Gamma^{\rm ano}(h \to X) = \frac{\Gamma^{\rm ano}(h \to X)}{\Gamma^{\rm SM}(h \to X)}\Big|_{\rm tree} \Gamma^{\rm SM}(h \to X)|_{\rm soa}, \tag{10}$$

where the SM result $\Gamma^{\rm SM}(h \to X)|_{\rm soa}$ is also obtained from Ref. [50]. The total width and branching ratios are evaluated following this recipe. We use the SM cross sections and decay widths and compute our predictions for $m_H = 125$ GeV. The observed Higgs boson mass by ATLAS (126.5 GeV) [7] and CMS (125.3 GeV) [8] are compatible within the experimental errors. We verified that the impact of changing the Higgs boson mass to 126.5 GeV is a subleading effect and does not alter our results. We did not include in our analyses an eventual invisible decay of the Higgs boson [51,52]; therefore, the total width is obtained by summing over the decays into the SM particles.

The search for the Higgs boson decaying into $b\bar{b}$ pairs takes place through Higgs boson production in association with a W or a Z so we can write

$$\mu_{b\bar{b}} = \frac{\sigma_{WH}^{\rm ano} + \sigma_{ZH}^{\rm ano}}{\sigma_{WH}^{\rm SM} + \sigma_{ZH}^{\rm SM}} \otimes \frac{{\rm Br}^{\rm ano}[h \to b\bar{b}]}{{\rm Br}^{\rm SM}[h \to b\bar{b}]} \tag{11}$$

with the superscript ano (SM) standing for the value of the observable considering the anomalous and SM interactions (pure SM contributions).

The CMS analyses of the 7 (8) TeV data separate the $\gamma\gamma$ final into five (six) categories, and the contribution of each production mechanism to a given category is presented in Table 2 of Ref. [25]. Therefore, we write the theoretical signal strength in these cases as

$$\mu_{\gamma\gamma}^{\rm CMS} = \frac{\epsilon_{gg}\sigma_{gg}^{\rm ano}(1+\xi_g) + \epsilon_{\rm VBF}\sigma_{\rm VBF}^{\rm ano} + \epsilon_{\rm VH}(\sigma_{WH}^{\rm ano} + \sigma_{ZH}^{\rm ano}) + \epsilon_{t\bar{t}H}\sigma_{t\bar{t}H}^{\rm ano}}{\epsilon_{gg}\sigma_{gg}^{\rm SM} + \epsilon_{\rm VBF}\sigma_{\rm VBF}^{\rm SM} + \epsilon_{\rm VH}(\sigma_{WH}^{\rm SM} + \sigma_{ZH}^{\rm SM}) + \epsilon_{t\bar{t}H}\sigma_{t\bar{t}H}^{\rm SM}} \otimes \frac{{\rm Br}^{\rm ano}[h \to \gamma\gamma]}{{\rm Br}^{\rm SM}[h \to \gamma\gamma]}, \tag{12}$$

where ξ_g is the pull associated with the gluon fusion cross section uncertainties, and the branching ratio and the anomalous cross sections are evaluated using the prescriptions (9) and (10). The weight of the different channels to each category is encoded in the parameters ϵ_X with $X =$ VBF, gg, VH, and $t\bar{t}H$ and they are presented in Tables III and IV.

[2]With the present statistics, our results are not sensitive to the theory pulls (see below), indicating that this approximation is reasonable for the time being.

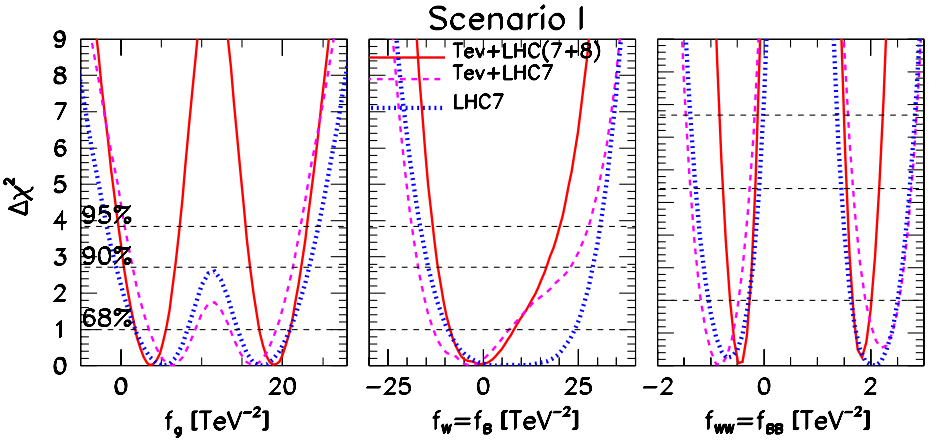

FIG. 1 (color online). The left (central, right) panel exhibits $\Delta\chi^2$ as a function of f_g (f_W, f_{WW}) in the framework of scenario I. Each panel contains three lines: the dotted (dashed) line was obtained using only the LHC 7 TeV (LHC 7 TeV and Tevatron) data while the solid line stands for the result using all the available data. In each panel, $\Delta\chi^2$ is marginalized over the two undisplayed parameters.

With the exception of the above processes, all other channels are treated as inclusive, so we write the expected signal strength of the final state F as

$$\mu_F = \frac{\sigma^{\rm ano}_{gg}(1+\xi_g) + \sigma^{\rm ano}_{\rm VBF} + \sigma^{\rm ano}_{WH} + \sigma^{\rm ano}_{ZH} + \sigma^{\rm ano}_{t\bar{t}H}}{\sigma^{\rm SM}_{gg} + \sigma^{\rm SM}_{\rm VBF} + \sigma^{\rm SM}_{WH} + \sigma^{\rm SM}_{ZH} + \sigma^{\rm SM}_{t\bar{t}H}} \otimes \frac{{\rm Br}^{\rm ano}[h \to F]}{{\rm Br}^{\rm SM}[h \to F]}. \quad (13)$$

Here we also use Eqs. (9) and (10) to obtain the anomalous cross sections and branching ratios.

For some final states, the available LHC 8 TeV data has been presented combined with the 7 TeV results. Given the limited available information on errors and correlations, we construct the expected theoretical signal strength as an average of the expected signal strengths for the center-of-mass energies of 7 and 8 TeV. We weight the contributions by the total number of events expected at each energy in the framework of the SM; i.e., given a final state X we evaluate

$$\mu^{\rm comb}_X = \frac{\mu^{7\,\rm TeV}_X \sigma^{\rm SM,7\,TeV}_X \mathcal{L}_{7\,\rm TeV} + \mu^{8\,\rm TeV}_X \sigma^{\rm SM,8\,TeV}_X \mathcal{L}_{8\,\rm TeV}}{\sigma^{\rm SM,7\,TeV}_X \mathcal{L}_{7\,\rm TeV} + \sigma^{\rm SM,8\,TeV}_X \mathcal{L}_{8\,\rm TeV}}, \quad (14)$$

where $\mathcal{L}_{7(8)\,\rm TeV}$ stands for the integrated luminosity at 7 (8) TeV accumulated in the channel being analyzed. When considering the full available data set, we consider all the processes in Tables I and II, neglecting the LHC 7 TeV processes whose data have been combined with the 8 TeV run; we indicate in Table II that the data have been combined by "@ 7 and 8 TeV."

The evaluation of the relevant tree level cross sections was done using the package MADGRAPH5 [53] with the anomalous Higgs boson interactions introduced using FEYNRULES [54]. We also cross checked our results using COMPHEP [55,56] and VBFNLO [57]. The evaluation of the partial width was done using the expressions presented in Ref. [32].

IV. CONSTRAINTS ON THE HIGGS BOSON ANOMALOUS INTERACTIONS

We next derive the allowed values of the Higgs boson interactions to vector bosons using the available Tevatron data [22], ATLAS 7 TeV [23,27] and 8 TeV [7,27] results, and CMS 7 TeV [24–26] and 8 TeV [8,25,26] data. The results are presented in Figs. 1–5, where several one-dimensional and two-dimensional projections of the $\Delta\chi^2 = \chi^2 - \chi^2_{\rm min}$ function(s) are shown. We find $\chi^2_{\rm min} = 12.12(12.13)$ in scenario I (II) for the global analysis (i.e., for a total number of 26 data points). The SM lays at $\chi^2_{\rm SM} = 20.87$, i.e., within the 96.7% (98.7%) CL region

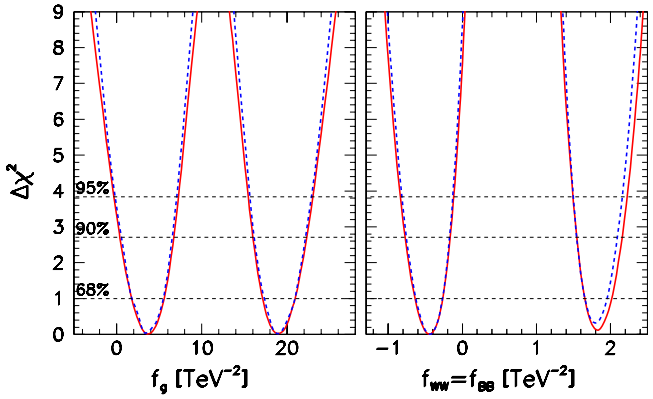

FIG. 2 (color online). $\Delta\chi^2$ as a function of f_g (left panel) and $f_{WW} = f_{BB}$ (right panel) for the full combined analysis. The solid lines correspond to scenario I, in which $\Delta\chi^2$ is marginalized over the two undisplayed parameters in each panel: $f_{WW} = f_{BB}$ and $f_W = f_B$ in the left panel, and f_g and $f_W = f_B$ in the right panel. The dashed lines correspond to scenario II, i.e., imposing first the prior $f_W = f_B = 0$ and then marginalizing over $f_{WW} = f_{BB}$ (left) and f_g (right).

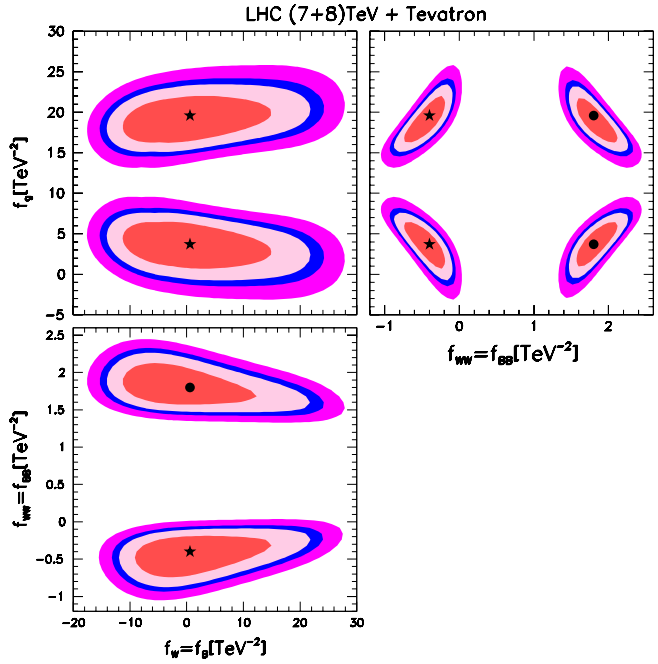

FIG. 3 (color online). 68, 90, 95, and 99% CL (2 dof) allowed regions of the plane $f_{WW} \otimes f_g$ (upper right panel), $f_W \otimes f_g$ (upper left panel) and $f_W \otimes f_{WW}$ (lower panel) using all available data. These results are obtained for scenario I and after marginalization over the undisplayed parameter in each panel. The best fit points are indicated by a star, while the second local minima are indicated with a dot.

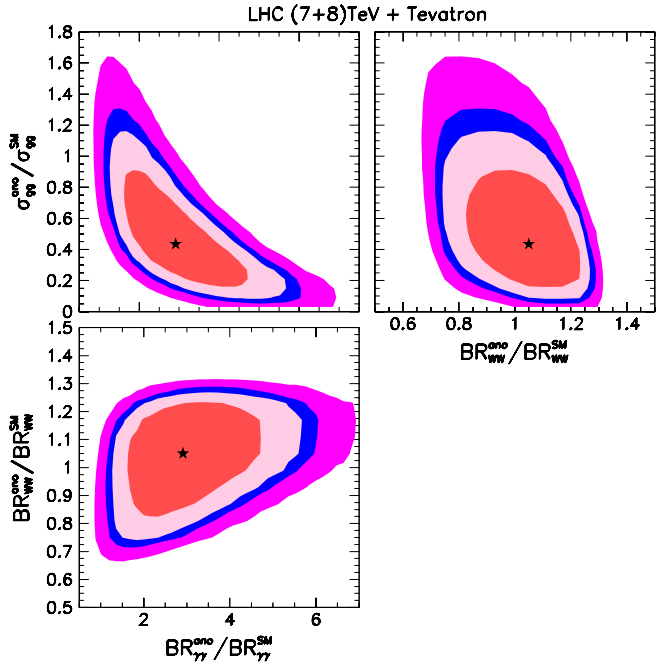

FIG. 5 (color online). Allowed regions for several combinations of Higgs boson branching ratios and production cross section. In each panel, $\Delta\chi^2$ is marginalized with respect to the combination of couplings independent of the two displayed observables. As in Fig. 3, the regions are shown at 68, 90, 95, and 99% CL (2 dof).

in the three-dimensional (two-dimensional) parameter space. The corresponding best fit values and 95% allowed ranges are summarized in Table V.

Figure 1 shows $\Delta\chi^2$ as a function of each of the operator coefficients in scenario I after marginalizing with respect to the two undisplayed ones. To illustrate the effect of the different data sets, the results are shown for three combinations of the available data: the dotted (dashed) line stands for the results obtained using only the LHC 7 TeV (LHC 7 TeV and Tevatron) data while the solid line is derived using the full available data set. The central panel of this figure displays the $\Delta\chi^2$ dependence on f_W. As we can see, the analysis of the LHC 7 TeV data only leads to a large flat region around the minimum, indicating that this

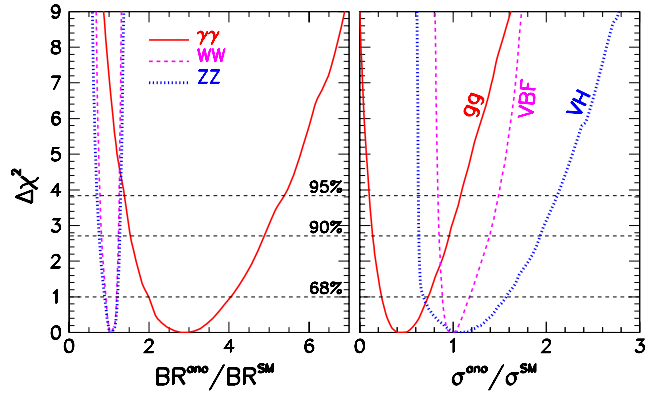

FIG. 4 (color online). $\Delta\chi^2$ as a function of Higgs boson branching ratios into electroweak gauge bosons (left panel) and the cross section for different production processes (right panel) normalized to the SM values. In the left panel, the solid (dashed, dotted) line stands for the branching ratio into $\gamma\gamma$ (W^+W^-, ZZ), while in the right panel, the solid (dashed, dotted) line represents the gluon fusion (VBF, VH) production cross section.

TABLE V. Best fit values and 95% CL allowed ranges for the combination of all available data. For f_g we show the two degenerate best fit values. For $f_{WW} = f_{BB}$ together with the best fit we show in parenthesis the value at the second minimum.

	Best fit	95% CL allowed range
$f_W = f_B$ (TeV^{-2})	-0.8	$[-13, 20]$
$f_{WW} = f_{BB}$ (TeV^{-2})	-0.4, (1.8)	$[-0.8, -0.1]$ and $[1.5, 2.2]$
f_g (TeV^{-2})	3.7, 19	$[-0.3, 7.3]$ and $[15, 23]$
$BR^{ano}_{\gamma\gamma}/BR^{SM}_{\gamma\gamma}$	2.9	[1.4, 5.4]
$BR^{ano}_{WW}/BR^{SM}_{WW}$	1.1	[0.8, 1.3]
$BR^{ano}_{ZZ}/BR^{SM}_{ZZ}$	1.1	[0.7, 1.3]
$\sigma^{ano}_{gg}/\sigma^{SM}_{gg}$	0.4	[0.1, 1.1]
$\sigma^{ano}_{VBF}/\sigma^{SM}_{VBF}$	1.0	[0.8, 1.5]
$\sigma^{ano}_{VH}/\sigma^{SM}_{VH}$	1.1	[0.6, 2.1]

data set has a small sensitivity to f_W, i.e., the Higgs boson couplings to W and Z pairs. This is expected since the $\gamma\gamma$ channel is the dominant observable in this sample. The addition of the Tevatron data, dominated by the Higgs boson associated production, enhances the sensitivity to deviations in HZZ and HW^+W^-, that is, to smaller values of f_W. The addition of the LHC 8 TeV results further tightens the allowed values, giving, for the global analysis, the constraint $-13 \leq f_W \leq 20$ at 95% CL.

$\Delta\chi^2$ as a function of f_g is shown in the left panel of Fig. 1 where we see that the analyses present two totally degenerate minima leading to two distinct allowed ranges. This degeneracy—as others that we encounter in this work—is due to the interference between the SM and anomalous contributions. We see that before the inclusion of LHC 8 TeV data, the two allowed ranges overlapped at CL higher than 90%, while in the global analysis they are separated at more than 3σ. The value of the gluon fusion cross section at the minima is around 43% of its SM value (see left panel of Fig. 4) and this cross section is highly suppressed in the region between the minima. This highly suppressed gluon fusion cross section was not completely disfavored before the 8 TeV data because the CDF and DØ and CMS @ 7 TeV $b\bar{b}$ channels still allowed for a larger f_W coupling to enhance associated production, compensating the large reduction of the gluon fusion cross section (see also discussion of Fig. 3). After the inclusion of the LHC 8 TeV data, this is no longer possible. So altogether the global analysis constrains f_g to lie in one of the two intervals $[-0.3, 7.3]$ or $[15, 23]$ at 95% CL.

The $\Delta\chi^2$ dependence on f_{WW} in scenario I is presented in the right panel of Fig. 1. A salient feature of this plot is that $\Delta\chi^2$ is concentrated around two narrow nonoverlapping regions centered around almost (but not totally) degenerate minima. Unlike for f_g, the two minima in $f_{WW} = f_{BB}$ are not fully degenerated because these operators modify not only the Higgs boson coupling to photons but also to WW and ZZ and the contributions to these last two vertices are slightly different at the two minima. Moreover, we also see that Tevatron data has a limited impact on this parameter, while the inclusion of the LHC 8 TeV results tighten the bounds on f_{WW} which at 95% CL is bounded to lie in one of the two intervals $[-0.8, -0.1]$ or $[1.5, 2.2]$.

The dependence on the scenario considered is illustrated in Fig. 2, where we plot the $\Delta\chi^2$ dependence on f_g and f_{WW} of the global analysis in scenarios I and II. As we can see, the results for both scenarios are almost coincident in both panels. This is due to the fact that in scenario I the full available data set is well described by $f_W = f_B \simeq 0$ for all allowed values of f_{WW} and f_g; consequently, the two scenarios give very similar results.

Let us turn our attention towards the correlations among the three free parameters of scenario I. Fig. 3 depicts 68, 90, 95, and 99% CL (2 dof) allowed regions of the $f_{WW} \otimes f_g$ (upper right panel), $f_W \otimes f_g$ (upper left panel), and $f_W \otimes f_{WW}$ (lower panel) planes using all attainable data. We obtained these plots by marginalizing over the free parameter not appearing in each of the panels.

We can see from the upper right panel of Fig. 3 that there are four well-isolated allowed *islands* in the $f_{WW} \otimes f_g$ plane. Moreover, within each of these islands, f_{WW} and f_g are strongly correlated or anticorrelated. As mentioned before, the existence of degenerate islands is due to the interference between the SM and anomalous contributions which allow two different values of the anomalous couplings to lead to the same cross section or branching ratio. In the case at hand, the gluon fusion cross section preferred by the fit is around 43% of its SM value. It is interesting to notice that if the results from the $b\bar{b}$ channel are removed from the fit, the vertical gap between the two islands on the left (or on the right) disappears—that is, intermediate values of f_g (which correspond to further suppressed gluon fusion production) become allowed. This happens because the $b\bar{b}$ data, which is dominated by associated production, constrains the coupling of the Higgs boson to W and Z pairs. In our framework, this leads to (a) an associated upper bound on the $H\gamma\gamma$ branching ratio, and (b) an upper bound on VBF and associated production. $\gamma\gamma$ data mainly restrict the product of the gluon fusion cross section and the Higgs boson branching ratio into photons; thus, weakening the upper bound on the latter allows the former to have smaller values. Furthermore, even smaller gluon fusion cross sections are permitted because of the possible increase in the VBF and associated production processes.

The upper left panel of Fig. 3 shows the presence of two isolated regions in the $f_W \otimes f_G$ plane and that there is a very weak correlation between the parameters within each region. Here again, the removal of the $b\bar{b}$ data leads to the disappearance of the gap between the allowed regions. The lower panel displays a behavior similar to the one observed in the upper left, but in the $f_W \otimes f_{WW}$ plane.

For the sake of completeness, we also show the results of the global analysis in scenario I in terms of the allowed ranges of Higgs boson production cross sections and decay branching ratios in Figs. 4 and 5. The results shown in these figures are obtained by projecting the three-dimensional $\Delta\chi^2$ function on the displayed observables and marginalizing on the independent undisplayed combination(s).

Finally, we also verified that the results do not change significantly when we do not employ the pulls to perform the fit. This behavior could be anticipated since the experimental errors are still much larger than the errors described by the pulls—a situation that will change as more statistics accumulate.

V. DISCUSSION

Once a Higgs boson—like state has been discovered, we must study its properties to establish if it is indeed the state predicted by the SM. In addition to that, it is also important

to look for additional states that might play a role in the electroweak symmetry breaking. In this article we have studied the Higgs boson couplings to gauge bosons using a model-independent characterization of the deviations with respect to the SM values in terms of dimension-six operators and the available data from Tevatron and LHC at 7 and 8 TeV. This approach still assumes that the Higgs boson field is a doublet of the $SU(2)_L$ symmetry and that the deviations of its couplings from the SM values are due to additional heavy states. Notwithstanding, our framework allows for independent modifications of the couplings to gluons, photons, and weak gauge bosons.

In this study we have demonstrated that the present available data are enough to start gaining some information on the different Higgs boson couplings to gauge bosons. For instance, our analyses indicate that a reduced gluon fusion cross section is preferred when we use the full available data set, with the most favored value being 43% of the SM value. We can see this preference for a reduced gluon fusion cross section in the right panel of Fig. 4, while the VBF and associated production cross sections are in agreement with the SM prediction. From this panel we can extract that the 95% CL allowed region of the gluon fusion cross section is [0.1, 1.1] times the corresponding SM value. This is consistent with the CMS analyses [8] which, using a different framework, also point in this direction, since a reduced coupling of the Higgs boson to top quarks is preferred by their results.

Taking into account that the presently measured $\gamma\gamma$ yield is above the SM prediction, the diminished gluon fusion cross section points to an enhanced Higgs boson branching ratio in $\gamma\gamma$; a fact that can be observed in our analyses. The left panel of Fig. 4 shows that the $\gamma\gamma$ branching ratio is indeed augmented, with a best fit value of 2.9 times the SM value and the 95% CL allowed region being [1.4, 5.4] times the SM branching ratio. Furthermore, we can see from this panel that the Higgs boson branching ratio into W^+W^- and ZZ is in agreement with the SM expectations.

Presently the $\gamma\gamma$ channel is the best measured channel and its rate is above the SM prediction. The operators $\mathcal{O}_{WW}$, $\mathcal{O}_{BB}$, and $\mathcal{O}_{GG}$ are the ones affecting this channel; therefore, they are the ones showing the largest impact of the full data set. This can be seen from the strong correlations and the well-isolated islands present in the upper right panel of Fig. 3, as well as by the correlations between the gluon fusion cross section and the Higgs boson branching ratios into electroweak gauge bosons in Fig. 5. From the upper left panel of this figure, we can see an anticorrelation between the gluon fusion cross section and the Higgs boson branching ratio into two photons; once again it is clear that there is a preference for reduced gluon fusion cross sections and enhanced decay into photon pairs. The other two panels of Fig. 5 show the mild dependence of the Higgs boson branching ratio into W^+W^- with the gluon fusion cross section or the two-photon branching ratio.

Our analyses of scenario I also show that the presently available data prefer small values of $f_W = f_B$; see the central panel of Fig. 1. This indicates that large deviations in HZZ and HW^+W^- interactions, as well as to triple gauge boson couplings, are not favored. This behavior was expected because the data points for Higgs boson couplings to W's and Z's are in agreement with the SM within 1σ; see Fig. 4, left panel. Furthermore, the present direct constraints on triple gauge boson vertices lead to bounds on f_W that are of the same order as the ones derived here from Higgs boson phenomenology. So, in the future, the combined analysis of Higgs boson data and measurements of the anomalous triple gauge boson couplings can be used to reduce the degeneracies observed in our results, since they present a different dependence on the anomalous couplings f_W and f_B; see Eqs. (4) and (6). In this respect, it is interesting to notice that electroweak precision measurements still give rise to the tightest limits on the Higgs boson anomalous interactions [30,34].

We finish with a word of warning. The precise numerical results presented here, that are summarized in Table V, should be taken with a grain of salt; due to the simplifying hypothesis used in our analyses, we should be aware that details can change if a more complete approach is used. Nevertheless, we verified that our results are rather robust when we use only parts of the available data.

ACKNOWLEDGMENTS

O. J. P. E. is grateful to the Institute de Physique Théorique de Saclay for its hospitality. O. J. P. E. is supported in part by Conselho Nacional de Desenvolvimento Científico e Tecnológico (CNPq) and by Fundação de Amparo à Pesquisa do Estado de São Paulo (FAPESP); M. C. G.-G. is also supported by USA-NSF Grant No. PHY-0653342, by CUR Generalitat de Catalunya Grant No. 2009SGR502 and together with J. G.-F. by MICINN FPA2010-20807 and consolider-ingenio 2010 program CSD-2008-0037. J. G.-F. is further supported by Spanish ME FPU Grant No. AP2009-2546. T. C. is supported by USA-NSF Grant No. PHY-0653342. O. J. P. E. is grateful to R. Zukanovich Funchal for enlightening discussions.

[1] F. Englert and R. Brout, Phys. Rev. Lett. **13**, 321 (1964).
[2] P. W. Higgs, Phys. Rev. Lett. **13**, 508 (1964).
[3] P. W. Higgs, Phys. Lett. **12**, 132 (1964).
[4] G. Guralnik, C. Hagen, and T. Kibble, Phys. Rev. Lett. **13**, 585 (1964).
[5] P. W. Higgs, Phys. Rev. **145**, 1156 (1966).
[6] T. Kibble, Phys. Rev. **155**, 1554 (1967).
[7] F. Gianotti (ATLAS Collaboration), http://indico.cern.ch/conferenceDisplay.py?confId=197461.
[8] J. Incandela (CMS Collaboration), http://indico.cern.ch/conferenceDisplay.py?confId=197461.
[9] For a recent review, see G. Altarelli, arXiv:1206.1476.
[10] S. Dimopoulos and L. Susskind, Nucl. Phys. **B155**, 237 (1979).
[11] S. Weinberg, Phys. Rev. D **19**, 1277 (1979).
[12] For a review, see C. T. Hill and E. H. Simmons, Phys. Rep. **381**, 235 (2003).
[13] D. B. Kaplan and H. Georgi, Phys. Lett. **136B**, 183 (1984).
[14] D. B. Kaplan, H. Georgi, and S. Dimopoulos, Phys. Lett. **136B**, 187 (1984).
[15] T. Banks, Nucl. Phys. **B243**, 125 (1984).
[16] M. J. Dugan, H. Georgi, and D. B. Kaplan, Nucl. Phys. **B254**, 299 (1985).
[17] H. Georgi, D. B. Kaplan, and P. Galison, Phys. Lett. **143B**, 152 (1984).
[18] K. Agashe, R. Contino, and A. Pomarol, Nucl. Phys. **B719**, 165 (2005).
[19] G. Giudice, C. Grojean, A. Pomarol, and R. Rattazzi, J. High Energy Phys. 06 (2007) 045.
[20] W. Buchmuller and D. Wyler, Nucl. Phys. **B268**, 621 (1986).
[21] C. N. Leung, S. Love, and S. Rao, Z. Phys. C **31**, 433 (1986).
[22] The TEVNPH Working Group for the CDF and D0 Collaborations, arXiv:1207.0449.
[23] G. Aad *et al.* (ATLAS Collaboration), Phys. Rev. D **86**, 032003 (2012).
[24] S. Chatrchyan *et al.* (CMS Collaboration), Phys. Lett. B **710**, 26 (2012).
[25] CMS Collaboration, Report No. CMS PAS HIG-12-015.
[26] CMS Collaboration, Report No. CMS PAS HIG-12-020.
[27] ATLAS Collaboration, Report No. ATLAS-CONF-2012-091.
[28] K. Hagiwara, S. Ishihara, R. Szalapski, and D. Zeppenfeld, Phys. Rev. D **48**, 2182 (1993).
[29] K. Hagiwara, R. Szalapski, and D. Zeppenfeld, Phys. Lett. B **318**, 155 (1993).
[30] K. Hagiwara, S. Matsumoto, and R. Szalapski, Phys. Lett. B **357**, 411 (1995).
[31] O. J. Eboli, M. Gonzalez-Garcia, S. Lietti, and S. Novaes, Phys. Lett. B **478**, 199 (2000).
[32] M. Gonzalez-Garcia, Int. J. Mod. Phys. A **14**, 3121 (1999).
[33] A. De Rujula, M. Gavela, P. Hernandez, and E. Masso, Nucl. Phys. **B384**, 3 (1992).
[34] S. Alam, S. Dawson, and R. Szalapski, Phys. Rev. D **57**, 1577 (1998).
[35] J. Espinosa, C. Grojean, M. Muhlleitner, and M. Trott, J. High Energy Phys. 05 (2012) 097.
[36] J. Ellis and T. You, J. High Energy Phys. 06 (2012) 140.
[37] D. Carmi, A. Falkowski, E. Kuflik, and T. Volansky, J. High Energy Phys. 07 (2012) 136.
[38] A. Azatov, R. Contino, and J. Galloway, J. High Energy Phys. 04 (2012) 127.
[39] M. Klute, R. Lafaye, T. Plehn, M. Rauch, and D. Zerwas, arXiv:1205.2699.
[40] P. P. Giardino, K. Kannike, M. Raidal, and A. Strumia, J. High Energy Phys. 06 (2012) 117.
[41] F. Bonnet, M. Gavela, T. Ota, and W. Winter, Phys. Rev. D **85**, 035016 (2012).
[42] C. Arzt, M. Einhorn, and J. Wudka, Nucl. Phys. **B433**, 41 (1995).
[43] G. Aad *et al.* (ATLAS Collaboration), arXiv:1205.2531.
[44] A. Martelli (CMS collaboration, and f. t. C. collaboration), arXiv:1201.4596.
[45] K. Hagiwara, R. Peccei, D. Zeppenfeld, and K. Hikasa, Nucl. Phys. **B282**, 253 (1987).
[46] K. Nakamura *et al.* (Particle Data Group), J. Phys. G **37**, 075021 (2010).
[47] O. Eboli, J. Gonzalez-Fraile, and M. Gonzalez-Garcia, Phys. Lett. B **692**, 20 (2010).
[48] G. Fogli, E. Lisi, A. Marrone, D. Montanino, and A. Palazzo, Phys. Rev. D **66**, 053010 (2002).
[49] M. Gonzalez-Garcia and M. Maltoni, Phys. Rep. **460**, 1 (2008).
[50] S. Dittmaier *et al.* (LHC Higgs Cross Section Working Group), arXiv:1101.0593.
[51] J. R. Espinosa, M. Muhlleitner, C. Grojean, and M. Trott, arXiv:1205.6790.
[52] M. Raidal and A. Strumia, Phys. Rev. D **84**, 077701 (2011).
[53] J. Alwall, M. Herquet, F. Maltoni, O. Mattelaer, and T. Stelzer, J. High Energy Phys. 06 (2011) 128.
[54] N. D. Christensen and C. Duhr, Comput. Phys. Commun. **180**, 1614 (2009).
[55] A. Pukhov *et al.*, arXiv:hep-ph/9908288.
[56] E. Boos *et al.* (CompHEP Collaboration), Nucl. Instrum. Methods Phys. Res., Sect. A **534**, 250 (2004).
[57] K. Arnold *et al.*, arXiv:1107.4038.